CO-Coverage-Dependent Oxygen Dissociation on Pt(111) Surface

Bin Shan,*,† Neeti Kapur,† Jangsuk Hyun,† Ligen Wang,† John B Nicholas,† and Kyeongjae Cho*,‡

Nanostellar Inc., 3696 Haven Ave, Redwood City, California 94063, and Department of Materials Science and Engineering and Department of Physics, University of Texas at Dallas, Richardson, Texas 75080

Received: October 3, 2008; Revised Manuscript Received: November 12, 2008

Oxygen dissociation is one of the most critical steps in the CO oxidation reaction on transition metal surfaces. It has been shown both experimentally and theoretically that oxygen dissociation on clean platinum (Pt) surface proceeds via a precursor-mediated reaction path, with negligible activation barrier. On the other hand, the oxygen dissociation pathway under diesel engine operating conditions, where the metal surface is packed with CO molecules, is understood less clearly. In this paper, we report density functional theory calculations for O_2 dissociation on Pt(111) in the presence of varying CO coverage. Classical Monte Carlo simulations have been used to get an estimate of coadsorbed CO and O_2 configurations. Oxygen molecular precursor states binding energies were found to shift up in energy with increasing CO coverage, with transition state energies and final product energies following the same trend. The dissociated product state becomes endothermic beyond a critical CO coverage of 0.44 monolayer, where oxygen dissociation is no longer energetically favored on Pt(111). The origin of the change in activation barrier can be attributed to the limited space available for oxygen dissociation and the lateral repulsion from neighboring CO molecules. A linear correlation exists between the oxygen dissociation barrier and the molecular precursor binding energy. These findings give useful insight into the CO oxidation mechanism under realistic diesel engine operating conditions.

Introduction

Platinum is one of the most active and widely used transition-metal catalysts for carbon monoxide oxidation. The Langmuir–Hinshelwood mechanism of CO oxidation on Pt(111) involves a few elementary steps, namely CO adsorption, desorption, and diffusion on the surface; molecular oxygen (O_2) dissociation to form atomic oxygen; and reaction of atomic oxygen with CO to form carbon dioxide.[1] Oxygen dissociation is a critical step, since this reaction is responsible for providing atomic oxygen for the subsequent CO oxidation steps. Due to this fundamental interest and technological importance, there have been many experimental and theoretical efforts toward a better understanding of the oxygen dissociation mechanism. Experimentally, investigations have been carried out to clarify the adsorption and dissociation processes of molecular oxygen on Pt.[2−9] Using techniques such as scanning tunneling microscopy and near edge X-ray-absorption spectroscopy, both physisorbed and chemisorbed molecular oxygen on Pt(111) have been observed.[2−4,7−9] The physisorbed species is principally observed at low temperatures, while only the chemisorbed species is observed at temperatures above 40 K.[2] The molecular chemisorption state can be either from the interconversion of physisorbed states or from activated adsorption,[2,3] and the thermal activation of those states is believed to be the primary source for providing dissociated oxygen atoms in CO oxidation.[2,3,10,11] Direct dissociative chemisorption from the gas phase to dissociated oxygen atoms can play at most a very minor role.[3] Theoretically, Hafner et al. investigated the role of oxygen molecular precursor states (MPS) in the oxygen dissociation reactions on a variety of transition-metal surfaces.[10,11] These studies also conclude that oxygen dissociations on Pt, Pd, and Ni surfaces are all precursor-mediated, with negligible activation barriers with respect to the gas phase. Theoretical studies have also explored the oxygen dissociation path on alloy surfaces such as Pt−Co and Pt−Fe,[12] as well as dissociation on steps, defect sites, where undercoordinated metal atoms result in strongly bound species and high reactivity.[13,14]

The dissociation route from the molecular chemisorption precursor state to atomic oxygen is less clear when we have other adsorbates on the surface prior to oxygen dissociation, since the lateral interactions between molecules tend to alter the reaction kinetics. Previous experimental studies by Ertl et al. show that, even in the absence of other molecular species, O_2 dissociation is affected by the oxygen atoms in the vicinity from prior dissociation steps.[4] In diesel engine catalysis under cold start conditions, the catalyst surface is generally poisoned by CO.[15,16] Thus, at the initial low temperature stage of operation, O_2 dissociation takes place on a surface saturated with CO. In order to gain insight into the effects of coadsorbed CO molecules on the oxygen dissociation pathway on Pt(111), we have performed density functional theory (DFT) calculations[17] with the NEB method to locate the transition states (TS).[18] Monte Carlo (MC) simulations with realistic lateral interaction parameters have also been used to determine the CO and O_2 coadsorbed geometries. On the basis of our simulation results, we show that there is a repulsive effect of adsorbed CO molecules on the oxygen binding on the surface, with the energy of product states (two dissociated atomic oxygen) being most sensitive to neighboring CO molecules. The net effect of the CO presence accumulates in the activation barrier for O_2 dissociation. With increasing CO coverage, the overall oxygen dissociation route becomes energetically unfavorable beyond a critical CO coverage. The branching ratio of dissociation to

* To whom correspondence should be addressed. E-mail: bshan@nanostellar.com (B.S.), kjcho@utdallas.edu (K.C.).
† Nanostellar Inc.
‡ University of Texas at Dallas.

10.1021/jp808763h CCC: $40.75
Published on Web 12/18/2008

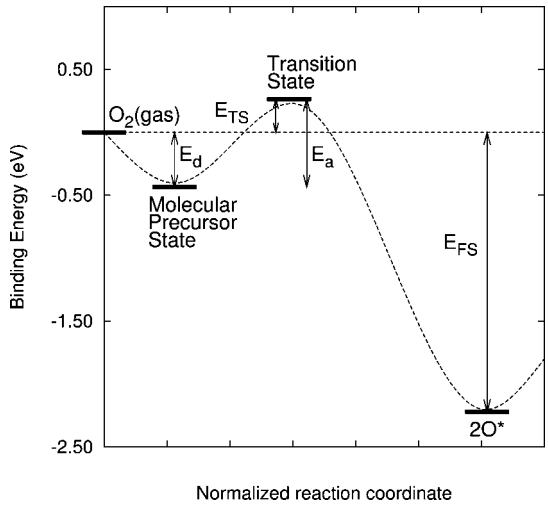

Figure 1. Schematic energy diagram for oxygen dissociation on a transition-metal surface.

TABLE 1: Parameters for the Monte Carlo Simulations

binding energies on clean Pt(111)				
CO	ΔE_{top}	ΔE_{bridge}	ΔE_{fcc}	ΔE_{hcp}
E_{ads}(eV)	−1.442	−1.429	−1.433	−1.395
O_2	$\Delta E_{t\text{-}f\text{-}b}$	$\Delta E_{t\text{-}b\text{-}t}$	$\Delta E_{t\text{-}h\text{-}b}$	
E_{ads}(eV)	−0.449	−0.432	−0.285	
lateral interactions				
CO−CO	$\alpha = 0.292$ eV, $\beta = 2.976$ Å^{-1}			
O_2−CO	$\alpha = 0.319$ eV, $\beta = 2.805$ Å^{-1}			

desorption is more sensitive to CO coverage as compared to local activation barrier. Our calculations offer a new perspective on the CO oxidation reaction under realistic diesel engine operating conditions.

Computational Methods

In order to model the CO and O_2 coadsorption pattern and explore the O_2 dissociation path on Pt(111), we have used a $(2\sqrt{3} \times 4)$ supercell with 16 Pt atoms per layer. The metal slab consists of three layers, with the bottom layer fixed at its crystallographic bulk lattice positions, and the rest of the atoms free to relax in all directions. A vacuum layer of 11 Å has been introduced to eliminate image interactions. One oxygen molecule and incremental numbers of CO (up to 0.44 ML) were adsorbed on the surface within the unit cell and allowed to equilibrate.

Self-consistent DFT calculations were carried out with revised Perdew−Burke−Ernzerhof (RPBE) generalized gradient correction for the exchange-correlation functional, which has been shown to give accurate values for adsorption energies of many molecular species.[19] The Vienna ab initio simulation package was used for the calculations.[20] The Kohn−Sham single electron wave function was expanded by plane waves with an energy cutoff of 400 eV, and this cutoff energy gives a good convergence for both adsorption energies and activation barriers. A $4 \times 4 \times 1$ k point mesh was used to sample the first Brillouin zone. The geometry optimization was terminated when the Hellmann−Feynman force on each atom was less than 0.05 eV/Å. The adsorption energy is calculated using the following equation:

$$\Delta E_{ads} = E_{total} - E_{sub} - E_{mol} \quad (1)$$

where E_{tot}, E_{sub}, and E_{mol} refer to the energies of the total system, the substrate, and the molecule, respectively. The minimum

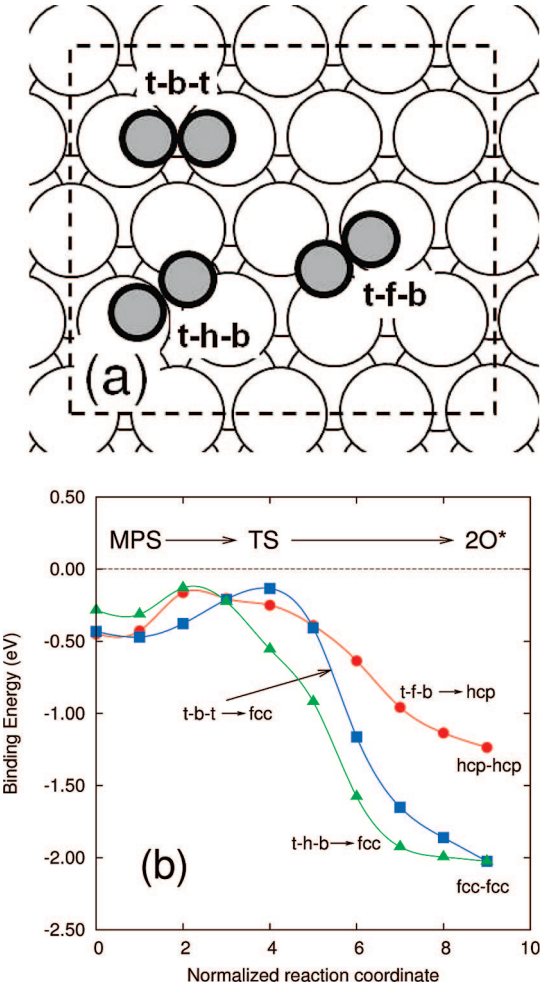

Figure 2. (a) Stable adsorption geometries for O_2 molecule on a clean Pt(111) surface in t-f-b, t-b-t, and t-h-b positions, respectively. Large circles represent Pt atoms and small gray circles represent oxygen atoms. The simulation unit cell is also indicated by the dotted square. (b) Minimum-energy pathways for O_2 dissociation on a clean Pt(111) surface to oxygen atoms from different precursor states.

energy reaction path for oxygen dissociation on clean and CO-covered Pt(111) surface was obtained by the NEB method.[18] Eight intermediate images were used to interpolate the reaction path between the fixed reactant state and product state. Once a minimum-energy path is converged, the apparent activation barrier for oxygen dissociation can be readily determined from the energy of the highest image along the path. The energy values are reported with respect to gas phase O_2.

To get a reasonable representation of the coadsorbed CO and O_2 geometries, MC simulations with parametrized CO−CO and CO−O_2 lateral interactions were used to equilibrate the surface.[21] Lateral interactions between molecules were fitted to a few selected CO and O_2 coadsorption configurations. An exponential functional term had been used to describe the repulsive interactions between the molecules. Within this formalism, the total energy of the system can be written as

$$E_{sys} = \sum_i \Delta E_i^{CO} + \sum_j \Delta E_j^{O_2} + \frac{1}{2}\sum_{l,m} \alpha \exp[-\beta(R_{lm} - r_0)] \quad (2)$$

where $\Delta E^{CO/O_2}$ represents the intrinsic molecular binding energies at different sites, and the third term is through-space interactions between adsorbates. R_{lm} is the distance between the

TABLE 2: Adsorption Energies for O_2 Molecular Precursor State, Transition State and Dissociated Atomic Oxygen[a]

					bond lengths in TS	
Pt (111)	O_2 MPS (eV)	dissociated atomic oxygen (eV)	E_{TS} (eV)	E_a (eV)	O−O (Å)	O−Pt[b] (Å)
t-f-b	−0.45	−1.23	−0.16	0.29	1.86	1.87 (T) 2.03 (B)
t-b-t	−0.43	−2.02	−0.13	0.30	1.88	1.84 (T) 1.99 (B)
t-h-b	−0.28	−2.02	−0.13	0.15	1.88	1.84 (T) 1.89 (B)

[a] Bond lengths of O−O and O−Pt for transition state are also included. [b] (T)/(B) stands for the distance between Pt and a top (T) or bridge (B) bonded oxygen, respectively.

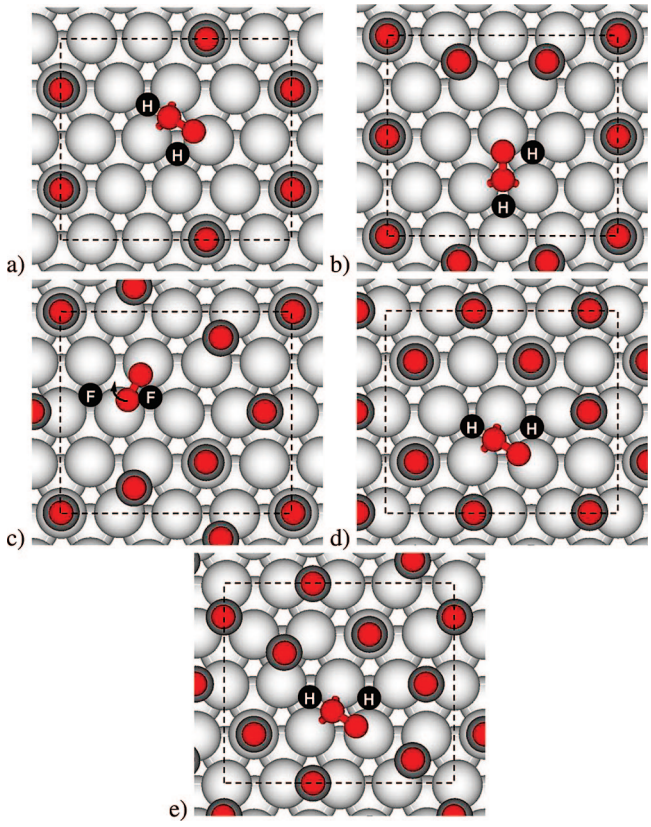

Figure 3. O_2 molecular precursor states with different CO coverage: (a) 0.19 ML, (b) 0.25 ML, (c) 0.31 ML, (d) 0.38 ML, and (e) 0.44 ML. Light gray circles represent Pt atoms, dark gray circles represent C atoms, and small red circles represent O atoms. Black dots with H/F indicate the position of the dissociated atomic oxygen in either hcp (H) or fcc (F) positions. The arrow in panel c indicates that the oxygen rotates from t-b-t to t-h-b before dissociation.

adsorbates l and m and r_0 is the equilibrium Pt lattice constant of 2.82 Å. Table 1 shows detailed parameters for binding energies as well as lateral interactions that were used in the MC simulations. The magnitude of the fitted lateral interactions agree with those in previous literature.[26,22,23] With the binding energies and lateral interactions setup, we deposited an initial random configuration of one oxygen molecule plus N number of CO molecules ($N = 3, 4, 5, 6, 7$) on the ($2\sqrt{3} \times 4$) metal surface. A periodic boundary condition was invoked and each molecule feels interactions from all neighboring molecules within a cutoff distance of 6 Å. The molecules were then allowed to hop among different sites and equilibrate themselves on the surface. CO molecules can occupy either top, bridge, face-centered cubic (fcc), or hexagonal close-packed (hcp) sites, while O_2 molecule can adsorb on a t-f-b, t-b-t, or t-h-b position (see Figure 2). The total energy of the system was evaluated after each molecular movement and the new configuration was accepted or rejected using the Metropolis algorithm.[24] Each simulation is run for 1 million steps, during which multiple temperature ramps, including heating up and cooling down, between 10 and 2000 K, is carried out to avoid trapping of the configuration in its local minima. The coadsorbed pattern with the lowest total system energy was recorded and used in the subsequent DFT calculations to study the oxygen dissociation and elucidate the relationship between O_2 dissociative adsorption and CO coverage.

Results and Discussions

Several key binding energy values as outlined in Figure 1 characterize the energetics of oxygen dissociation. E_d represents the desorption energy of oxygen MPS and dictates the lifetime of oxygen MPS on the surface. E_a is the local activation barrier for dissociation of MPS to atomic oxygens, and E_{FS} represents the overall reaction enthalpy. The other essential energetic parameter in oxygen dissociation is the apparent activation barrier, namely, the transition state energy E_{TS} with respect to gas phase O_2 molecular energy. Consider the case where adsorbed O_2 is in equilibrium with the gas phase, the probability of dissociation (with a barrier of E_a) must be compete with the probability of desorption (with a barrier of E_d). The branching ratio between these two events depends exponentially on the difference between E_a and E_d, which equals E_{TS}. Thus, E_{TS} is also an important quantity in describing the local reactivity of oxygen dissociation under different environments.

In this paper, a general picture of the stability of oxygen MPS and dissociated atomic oxygen as a function of CO coverage will be presented in the first part of this section. We then study in detail the activation barrier and reaction path for oxygen dissociation in the presence of coadsorbed CO molecules. Considerable increase in E_{TS} is observed, while E_a remains approximately constant. The potential implications of the results are discussed in the context of diesel engine catalysis.

O_2 Precursor State and Dissociation on Clean Pt (111) Surface. Both theoretical and experimental evidence indicates the existence of a molecular oxygen precursor state on a clean platinum surface.[4,7−11] We have adsorbed O_2 molecule on a clean Pt(111) surface at different sites and with different orientations. After optimization, three stable O_2 precursor states were identified. Figure 2a shows the energetically favorable configurations for O_2 MPS. Among the three possible configurations, the O_2 precursor with t-f-b adsorption geometry has the strongest adsorption energy of −0.45 eV. Within DFT accuracy, t-f-b and t-b-t adsorption geometries are energetically degenerate. The calculated precursor adsorption energies are in good agreement with experimental estimates of −0.4 to −0.5 eV.[25,26] The O_2 MPS occupying t-f-b and t-h-b configurations show zero magnetic moments, while t-b-t adsorption states carry a net magnetic moment of 0.77 μ_b. During MC simulations for CO

TABLE 3: Adsorption Energies of O_2 Molecular Precursor State, Transition State, and Dissociated Oxygen Atoms on Clean Surface and with Various CO Coverages[a]

					bond lengths in TS	
CO coverage (ML)	O_2 MPS (eV)	dissociated atomic oxygen (eV)	E_{TS} (eV)	E_a (eV)	O−O (Å)	O−Pt (Å)[b]
0 (clean)	−0.45	−1.23	−0.16	0.29	1.86	1.87 (T) 2.03 (B)
0.19	−0.31	−0.96	−0.03	0.28	1.84	1.88 (T) 2.03 (B)
0.25	−0.33	−0.70	+0.03	0.36	1.90	1.87 (T) 2.02 (B)
0.31	−0.22	−1.41	+0.18	0.40	1.71	1.95 (T) 2.08 (B)
0.38	−0.14	−0.39	+0.13	0.27	1.89	1.88 (T) 2.02 (B)
0.44	−0.02	+0.06	+0.33	0.35	2.04	1.87 (T) 2.01 (B)

[a] The bond lengths of O−O and O−Pt of the transition state are included. [b] (T)/(B) stands for the distance between Pt and a top/bridge bonded oxygen, respectively.

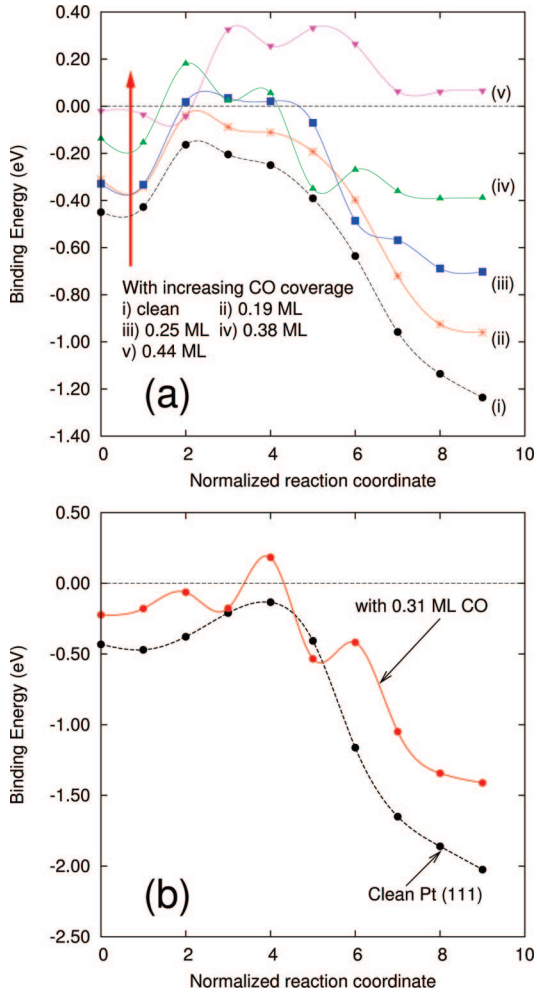

Figure 4. (a) O_2 dissociation path from t-f-b MPS to two hcp-adsorbed oxygen atoms as a function of increasing CO coverage. (b) O_2 dissociation path from t-b-t MPS to two fcc-adsorbed oxygen atoms with 0.31 ML of CO coverage. Dotted lines indicate their corresponding paths on clean Pt(111).

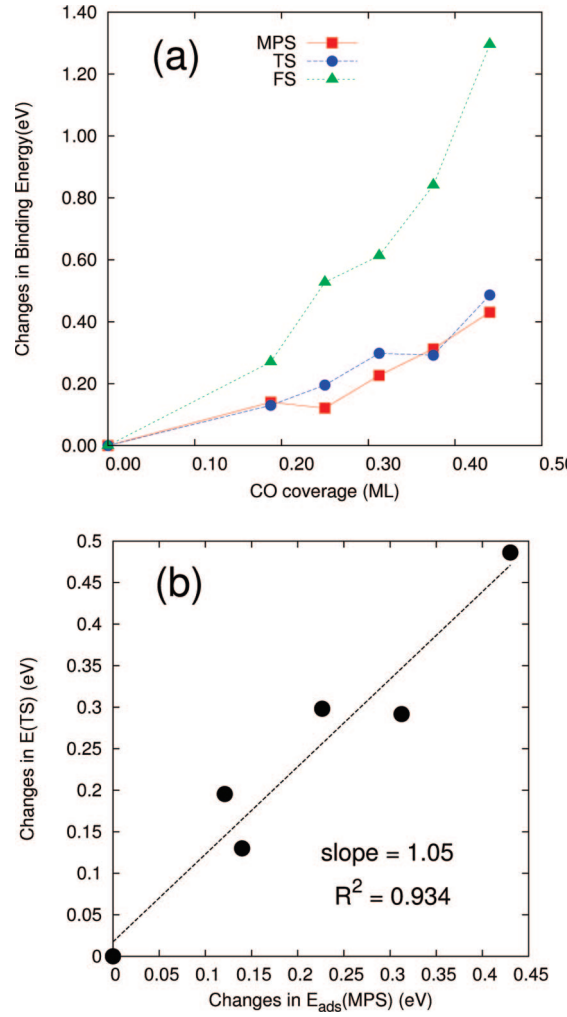

Figure 5. (a) Binding energy trends for MPS, TS, and FS with increasing CO coverage. (b) Correlation between the increase in energies of O_2 MPS and TS. The binding energies of different species on the clean surface are set to zero.

and O_2 coadsorbed surface, t-f-b and t-b-t are the observed adsorption geometries. The t-h-b geometry does not appear in coadsorption geometries, because it is less stable than the other two MPS by more than 0.15 eV.

Next, we have studied the O_2 dissociation path on the clean Pt(111) surface, in which O_2 in t-f-b dissociates into two hcp-adsorbed oxygen atoms, while O_2 in t-b-t and t-h-b configurations dissociates into two atomic oxygens at fcc sites. Figure 2b depicts the minimum-energy paths determined by nudged elastic band (NEB) calculations. For the dissociation path starting from O_2 in t-f-b and t-h-b, the oxygen dissociation barrier is slightly lower than the desorption barrier, which agrees well with experiments.[2] The transition state for these two paths are also similar, with one oxygen at an off-top position and the

other oxygen on a bridge position. The energetic and geometrical parameters of the transition states are listed in Table 2. For the dissociation starting from O_2 in t-b-t, the t-b-t MPS first rotate into t-h-b position, due to the small rotational barrier between them,[10] and then undergo the same dissociation route as starting from t-h-b. It is worth noting that the dissociated oxygen atoms residing on two neighboring sites still feel lateral interactions of around 0.1 eV due to metal-sharing effect. The energies of two adjacent fcc (hcp) adsorbed oxygen atoms are 2.02 eV (−1.23 eV), as compared to the energies of −2.2 eV (−1.30 eV) for two isolated atomic oxygens in fcc (hcp) sites on Pt(111). The repulsion is also manifested in the longer O−O distance observed as compared to the Pt lattice constant.

O_2 Molecular Precursor State with Coadsorbed CO. We studied the O_2 precursor state with three, four, five, six, and seven CO molecules in the $(2\sqrt{3} \times 4)$ unit cell, which corresponds to a local CO coverages of 0.19, 0.25, 0.31, 0.38. and 0.44 ML, respectively. The adsorption patterns of coadsorbed O_2 and CO obtained from the MC simulations are shown in Figure 3. Due to the repulsive interactions between CO−CO and CO−O_2 molecules, the adsorbates tend to form a relatively uniform distribution rather than clustering on the surface. The oxygen MPS were all found to be either in t-f-b or t-b-t positions due to stronger binding energy on those sites.

Table 3 lists the adsorption energies of O_2 MPS on Pt(111) with different amounts of CO coverage. It can be seen from the tabulated energies that as we increase the CO coverage, the O_2 molecular precursor energy gradually decreases, indicating that the surrounding CO has a strong influence on the adsorption of O_2 MPS. Figure 5 shows the increase of energy in O_2 MPS versus the CO coverage.

O_2 Dissociation on CO Covered Surface. The dissociation paths for the O_2 MPS to dissociated atomic oxygens, occupying two neighboring 3-fold sites, are shown in Figure 3. Since CO−O_2 coadsorption geometries involve mostly molecular oxygen in the t-f-b position, we illustrate the CO-dependent oxygen dissociation barrier by considering the path from t-f-b MPS to two hcp-adsorbed atomic oxygens. This particular dissociation path involves the breaking of the O−O bond, while one atomic oxygen simultaneously migrates toward an hcp site via an atop site and the other oxygen remains almost on the bridge site during the transition state. Some key parameters for the detailed transition state, including the O−O and O−Pt bond lengths, are listed in Table 3.

In Figure 4, reaction paths connecting the O_2 precursor state, transition state, and final state (FS) are plotted for increasing CO coverage. The O_2 molecular precursor state is initially stable with an adsorption energy of −0.45 eV, and there is no apparent activation barrier for O_2 dissociation. As we gradually increase the CO coverage, the MPS energy rises with respect to O_2 in the gas phase and becomes very weakly bound when CO coverage reaches 0.44 ML. The transition state energy also rises with comparable magnitude, and at 0.25 ML of CO, the apparent activation barrier (E_{TS} defined in Figure 1) is above zero, at which point oxygen dissociation is less favorable than desorption. The final state energy follows similar trends, except that the change in the final state energies is even more pronounced with increasing CO coverage. Due to the complex nature of the interactions between neighboring CO's, multiple local minima can exist in the reaction path. This is in contrast to the clean surface case, where a well-defined and energetically distinguished initial state and final state can be identified.

The coadsorption geometry with 0.31 ML of CO involves the t-b-t MPS as the initial state for O_2 dissociation and two fcc-adsorbed oxygen atoms as the final state. Similar to the O_2 (t-b-t) to 2O* (fcc−fcc) dissociation on a clean surface, the breaking of the O−O bond does not commence until the oxygen molecule is rotated into the t-h-b position, as depicted in Figure 4b.

Figure 5a summarizes the increase in binding energy for MPS, TS, and FS as a function of CO coverage, respectively. Clearly, the energy of dissociated oxygen is most sensitive to CO coverage, and there is a linear correlation between the transition state energy and the O_2 precursor energy, as demonstrated by Figure 5b. This is because the transition state geometry of oxygen dissociation is very close to the initial state as shown in Figure 4. Similar relationships have also been found for the elementary CO oxidation step, where the reaction barriers are mainly determined by the initial state energies.[27−29] It is also worth noting that while the variation in E_a (i.e., MPS activation energy barrier) under different neighboring CO environment is only around 0.1 eV, the E_{TS} varies as much as 0.5 eV. This indicates that the intrinsic dissociation rate change from O_2 MPS to atomic oxygen is not the most influential factor in determining the overall O_2 activation on CO-covered Pt(111). Our calculation shows that the most pronounced effect of CO coverage is the resulting change in branching ratio between oxygen dissociation and oxygen desorption from the MPS. Under CO coverage conditions, most of the adsorbed O_2 MPS would go back to the gas phase before dissociation, thus lowering the overall reactivity of oxygen dissociation.

From the above analysis, we can conclude that O_2 activation on Pt(111) is a strong function of CO coverage. With increasing CO coverage, the decreased branching ratio of O_2 dissociation and desorption decreases oxygen reactivity. Beyond the CO coverage of 0.44 ML, the dissociation of oxygen becomes endothermic. This indicates that the well-known Langmuir−Hinshelwood mechanism for CO oxidation might not hold for CO oxidation under high pressure, and some alternative reaction channel might play an important role. One possibility is that the dissociation of oxygen at high CO coverage involves step sites, since those coordinately unsaturated sites tend to facilitate the dissociation of oxygen molecules.[30] Another possibility could be that an alternative oxidation channel such as direct reactions of O_2 molecule with adsorbed CO becomes more preferrable as compared to the reaction route that involves oxygen dissociation.[3,31−33]

Conclusions

The reaction path for O_2 dissociation on Pt(111) surface under different CO coverage conditions has been studied using periodic self-consistent DFT (GGA-RPBE) calculations. MC simulations had been used to generate realistic CO and O_2 coadsorbed geometries. Despite the negligible apparent oxygen dissociation barrier on clean Pt(111) surface, a considerable barrier develops when the surface is packed with CO molecules. The energies of O_2 precursor state, transition state, and dissociated oxygen atoms all become less stable with increasing CO coverage. While the local activation barrier (E_a in Figure 1) remains roughly constant, the apparent activation barrier (E_{TS}) increases substantially in energy, leading to a large drop in branching ratio between oxygen dissociation and desorption and the resulting lower reactivity of oxygen dissociation. The reaction enthalpy of oxygen dissociation changes from exothermic to endothermic beyond a critical CO coverage of 0.44 ML. Our results provide useful insight into the effect of CO molecules on the O_2 dissociation energetics and pathways and their potential implications in CO oxidation kinetics.

Acknowledgment. We thank Prof. Matt Neurock, and Prof. Enrique Eglesia for fruitful discussions.

References and Notes

(1) Campell, C.; Ertl, G.; Kuipers, H.; Segner, J. *J. Chem. Phys.* **1980**, *73*, 5862–73.
(2) Luntz, A. C.; Grimblot, J.; Fowler, D. E. *Phys. Rev. B* **1989**, *39*, 12903–12906.
(3) Rettner, C. T.; Mullins, C. B. *J. Chem. Phys.* **1991**, *94*, 1626–35.
(4) Zambelli, T.; Barth, J. V.; Wintterlin, J.; Ertl, G. *Nature* **1997**, *390*, 495–7.
(5) Janin, E.; von Schenck, H.; Göthelid, M.; Karlsson, U. O.; Svensson, M. *Phys. Rev. B* **2000**, *61*, 13144–13149.
(6) Rose, M. K.; Borg, A.; Dunphy, J. C.; Mitsui, T.; Ogletree, D. F.; Salmeron, A. *Surf. Sci.* **2004**, *561*, 69–78.
(7) Stöhr, J.; Gland, J. L.; Eberhardt, W.; Outka, D.; Madix, R. J.; Sette, F.; Koestner, R. J.; Doebler, U. *Phys. Rev. Lett.* **1983**, *51*, 2414–2417.
(8) Outka, D. A.; Stöhr, J.; Jark, W.; Stevens, P.; Solomon, J.; Madix, R. J. *Phys. Rev. B* **1987**, *35*, 4119–4122.
(9) Wurth, W.; Stöhr, J.; Feulner, P.; Pan, X.; Bauchspiess, K. R.; Baba, Y.; Hudel, E.; Rocker, G.; Menzel, D. *Phys. Rev. Lett.* **1990**, *65*, 2426–2429.
(10) Eichler, A.; Mittendorfer, F.; Hafner, J. *Phys. Rev. B* **2000**, *62*, 4744–4755.
(11) Gross, A.; Eichler, A.; Hafner, J.; Mehl, M. J.; Papaconstantopoulos, D. A. *Surf. Sci.* **2003**, *539*, L542–8.
(12) Xu, Y.; Ruban, A. V.; Mavrikakis, M. *J. Am. Chem. Soc.* **2004**, *126*, 4717–4725.
(13) Li, T.; Balbuena, P. B. *Journal of Physical Chemistry B* **2001**, *105*, 9943–9952.
(14) Sljivancanin, Z.; Hammer, B. *Surf. Sci.* **2002**, *515*, 235–244.
(15) Longwitz, S. R.; Schnadt, J.; Vestergaard, E. K.; Vang, R. T.; Laegsgaard, E.; Stensgaard, I.; Brune, H.; Besenbacher, F. *J. Phys. Chem. B* **2004**, *108*, 14497–14502.
(16) Petrova, N. V.; Yakovkin, I. N. *Surf. Sci.* **2002**, *519*, 90–100.
(17) Kohn, W. *Rev. Mod. Phys.* **1999**, *71*, 1253–1266.
(18) *Classical and Quantum Dynamics in Condensed Phase Simulations*; Berne, B. J., Ciccotti, G., Coker, D. F., Eds.; World Scientific: Singapore, 1998.
(19) Hammer, B.; Hansen, L. B.; Nørskov, J. K. *Phys. Rev. B* **1999**, *59*, 7413–7421.
(20) Kresse, G.; Furthmuller, J. *Comput. Mater. Sci.* **1996**, *6*, 15–50.
(21) Shan, B.; Wang, L.; Hyun, J.; Yang, S.; Zhao, Y.; Nicholas, J. *MRS Proceedings*; San Francisco, CA, 2008.
(22) Nagasaka, M.; Kondoh, H.; Nakai, I.; Ohta, T. *J. Chem. Phys.* **2007**, *126*, 44704–1.
(23) Jansen, A. P. J.; Offermans, W. K. *Proceedings of the International Conference on Computational Science and Its Applications—ICCSA 2005*; Part I, 9−12 May 2005, Singapore, 2005; pp 1020−9.
(24) Metropolis, N.; Rosenbluth, A. W.; Rosenbluth, M. N.; Teller, A. H.; Teller, E. *J. Chem. Phys.* **1953**, *21*, 1087–1092.
(25) Lehwald, S.; Ibach, H.; Steininger, H. *Surf. Sci.* **1982**, *117*, 342–51.
(26) Gland, J. L.; Sexton, B. A.; Fisher, G. B. *Surf. Sci.* **1980**, *95*, 587–602.
(27) Liu, Z. P.; Hu, P. *Top. Catal.* **2004**, *28*, 71–78.
(28) Liu, Z. P.; Hu, P. *J. Chem. Phys.* **2001**, *115*, 4977–4980.
(29) Norskov, J. K.; Bligaard, T.; Logadottir, A.; Bahn, S.; Hansen, L. B.; Bollinger, M.; Bengaard, H.; Hammer, B.; Sljivancanin, Z.; Mavrikakis, M.; Xu, Y.; Dahl, S.; Jacobsen, C. J. H. *J. Catal.* **2002**, *209*, 275–278.
(30) Gee, A. T.; Hayden, B. E. *J. Chem. Phys.* **2000**, *113*, 10333–10343.
(31) Molina, L.; Hammer, B. *J. Chem. Phys.* **2005**, *123*, 161104.
(32) Cant, N. W.; Hicks, P.; Lennon, B. *J. Catal.* **1978**, *54*, 372–383.
(33) Conrad, H.; Ertl, G.; Kuppers, J. *Surf. Sci.* **1978**, *76*, 323–342.

JP808763H